Acta Montanistica Slovaca
ISSN 1335-1788
actamont.tuke.sk

# Determining the pressure increase in the hydraulic cylinders of powered roof support based on actual measurements

*Dawid SZURGACZ[1,2], Konrad TRZOP[3], Anthony J. S. SPEARING[4], Jiří POKORNY[5] and Sergey ZHIRONKIN[6,7]**

**Authors' affiliations and addresses:**
[1] Center of Hydraulics DOH Ltd., 41-906 Bytom, Poland;
e-mail: dawidszurgacz@vp.pl

[2] Polska Grupa Górnicza S.A., ul. Powstańców 30, 40-039 Katowice, Poland;
e-mail: dawidszurgacz@vp.pl

[3] KWK Ruda Ruch Bielszowice, ul. Halembska 160, 41-711 Ruda Slaska, Poland;
e-mail: konrad.trzop.kt@gmail.com

[4] School of Mines, China University of Mining and Technology, 1 Daxue Road, Tongshan District, Xuzhou 221116, China;
e-mail: sam.spearing@curtin.edu.au

[5] VSB - Faculty of Safety Engineering, Technical University of Ostrava, Lumírova 13/630, 700 30 Ostrava, Czech Republic;
e-mail: jiri.pokorny@vsb.cz

[6] Department of Trade and Marketing, Siberian Federal University, 79 Svobodny av., 660041 Krasnoyarsk, Russia;
e-mail: zhironkinsa@kuzstu.ru

[7] Department of Open Pit Mining, T.F. Gorbachev Kuzbass State Technical University, 28 Vesennya st., 650000 Kemerovo, Russia;
e-mail: zhironkinsa@kuzstu.ru

***Correspondence:**
Sergey Zhironkin, Department of Trade and Marketing, Siberian Federal University, 79 Svobodny av., 660041 Krasnoyarsk, Russia;
e-mail: zhironkinsa@kuzstu.ru

**How to cite this article:**
Szurgacz, D., Trzop, K., Spearing, A.J.S., Pokorny, J. and Zhironkin, S. (2022). Determining the pressure increase in the hydraulic cylinders of powered roof support based on actual measurements. *Acta Montanistica Slovaca*, Volume 27 (4), 876-891

**DOI:**
https://doi.org/10.46544/AMS.v27i4.04

## Abstract
Powered roof support in a longwall operation is designed to maintain a safe working area and allow the immediate roof to fail and collapse behind the support. The powered supports are loaded using large hydraulic pumps with non-return and preset-yielding valves. In addition to providing support to the immediate roof in the longwall production area, it also moves the armoured face conveyor and shearer forward as coal mining progresses. The research aimed to analyse the changes in the pressure values in the powered roof support section's hydraulic cylinders in relation to the occurrence of rock mass movements in the roof. The pressure measurements are based on the sensors in the sub-piston space of the powered roof support hydraulic prop located in the steel wall. The results allow a correlation to be developed between the roof movement and the loads generated in the hydraulic cylinders.

## Keywords
pressure measurement; hydraulic cylinder/prop; powered roof support; extraction wall; work safety; longwall mining

## Introduction

The development of technology related to monitoring machines and devices (Ziętek, et al., 2022; Bardzinski, et al., 2022; Bortnowski, et al., 2021) based on an innovative approach contributes to improving work safety (Zimroz, et al., 2021; Wang et al., 2021; Bazaluk, et al., 2021). Companies associated with underground mineral exploitation increasingly implement these solutions (Borkowski, et al., 2021; Jixiong, et al., 2017; Wajs, et al., 2021). The use of monitor systems contributes to increasing the efficiency of operation (Góralczyk, et al., 2020; Bazaluk, et al., 2021; Baiul, et al., 2020) of machines and devices (Krauze, et al., 2021; Qiao, et al., 2021; Wodecki, et al., 2020). This results in improved safety, increased productivity, and reduced working costs (Patyk, et al., 2021; Dlouhá, et al., 2019; Dlouhá and Kozlová, 2019). Nowadays, a lot of research is conducted in the mining field because of the ever-increasing need for materials and the more difficult mining conditions. The research addresses, among others, improving work safety (Ji, et al., 2020; Frith, et al., 2015), machine efficiency (Ralston, et al., 2015; Ralston, et al., 2017; Ren et al., 2021), and combating natural hazards (Pokorny, et al., 2018). In order to maintain the projected demand for hard coal as an energy raw material in the coming years, it will be important to research the ongoing development of existing coal mining technologies.

Using a monitoring system to measure the pressure in the hydraulic props of powered roof support in real conditions determines its basic operating parameters (Rajwa et al., 2019). These parameters include initial load capacity, working load capacity and nominal load capacity (Szurgacz, et al., 2021). Based on the pressure of the powered roof support, an analysis of the correctness of its operation can be carried out (Zhao, et al., 2015; Zhou, et al., 2022; Juárez-Ferreras, et al., 2008). The operation of the powered roof support is mainly influenced by roof deformation (both slow and rapid) caused by mining (Woźniak, et al., 2020; Bajda, et al., 2018; Kotwica, et al., 2021). Dynamic phenomena are caused by the exploitation depth and strength of surrounding rocks (Szurgacz, 2021; Klishin, et al., 2010; Ji, et al., 2016). Beyond this threat, the operation of the powered roof support takes place in the vicinity of associated hazards such as methane, the risk of gas and rock ejections (coal bumps or bursts), and many others that can be found in the literature (Mo, et al., 2019; Pokorny, et al., 2016; Dlouhá, et al., 2018). Seismic events within the rock mass have the most significant impact on the work of the powered roof support and pose the greatest threat to it (Xiaozhen, et al., 2012; Stoiński, et al., 2003). Powered roof support must be designed in such a way that it can react against this phenomenon and maintain overall stability (Kumar, et al., 2015). To prevent damage to the hydraulic cylinders, safety valves are incorporated into the hydraulic system (Buyalich, et al., 2017; Buyalich, et al., 2019). Their task is to rapidly release the excessive pressure in the piston space of the prop. In the steel longwall complex, the powered roof support is responsible for the safety of other equipment, specifically the armoured face conveyor and the shearer or plough (Hu, et al., 2018; Dlouhá, et al., 2021; Kotwica, et al., 2021). Their cooperation consists of the fact that the task of the shearer is to make coal and load it onto the conveyor (Gładysiewicz, et al., 2017; Bajda, et al., 2021; Szurgacz, et al., 2021). However, the role of the conveyor is the coal's transport (Kawalec, et al., 2020; Grzesiek, et al., 2021; Doroszuk, et al., 2019). Powered roof support is equipped with a hydraulic system that moves the machines mentioned above with operational progress (Huang, et al., 2019; Peng, et al., 2019, Bortnowski, et al., 2021). Figure 1 shows the view of the mining longwall face.

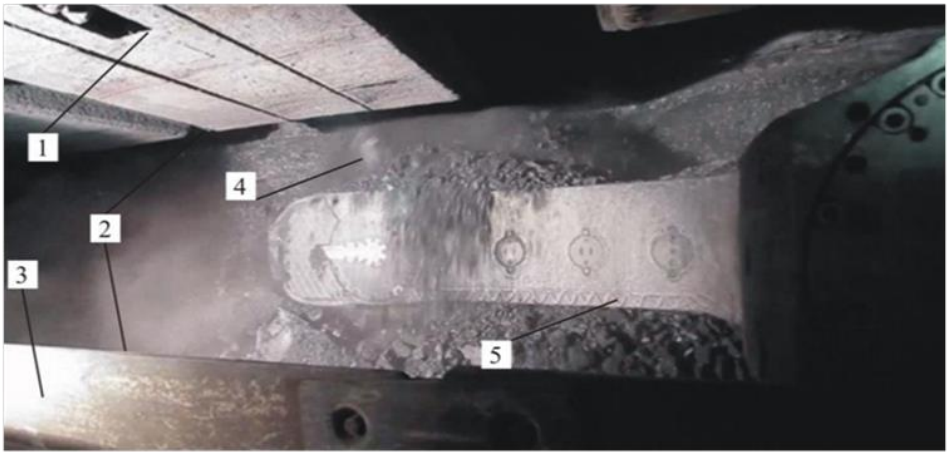


*Fig. 1. View of the extraction longwall of the Coal Mine, where: 1 – canopy of support section, 2 – excavated coalface, 3 – longwall conveyor extension, 4 – structured body, 5 – shearer's arm.*

This paper considers the analysis of changes in the pressure value in the sub-piston space of the powered roof support's hydraulic prop. The measurements were carried out in situ under normal operating conditions. The primary purpose of the research was to determine the pressure increase in the sub-piston space of the powered roof support based on the resulting rock mass shocks. In this respect, the analysis of changes taking place in the sub-

piston space of the prop was carried out. The study provided important information on the time at which changes in the powered roof support's work changes occur for the resulting dynamic phenomenon. The test results constitute essential information for the engineering and technical staff about the behaviour of the powered roof support during rock mass shock.

## Material and methods

Based on the reactive pressures measured (Tables 1 to 3) in the sub-piston space of the hydraulic prop of the powered roof support as a result of the dynamic rock mass shock, the average pressure of the liquid in the sub-piston space of the prop was determined, during the rapid rock mass movement, according to the proposed relations:

$$P_{av} = \frac{P_n + P_{max}}{2} \tag{1}$$

Where:
$P_n$ – nominal pressure of the safety valve,
$P_{max}$ – maximum pressure of the liquid in the under-piston space at the moment of rock mass shock

For the dependence mentioned above and measurement data included in Tables 1 to 3, the average pressure for the sub-piston space of the prop was determined. The nominal pressure for the safety valve was assumed to be 38MPa. The value of the adopted nominal pressure is the safety limit of the powered roof support. The results of this analysis are presented in Table 1 to Table 3 and illustrated in Figures 21-24.

The longwall excavation, in which the tests determining the pressure increase in the powered roof support prop were carried out, was located at a depth of 840 m. The height of the wall excavation is about 3 m. The length of the wall was about 252 m. The wall had 164 sections of the powered roof support type ZRP-15/35-POz. The longitudinal slope in the wall ranged from 0° to 10°, while the transverse slope ranged from 0° to 15°. The longwall was adversely affected by rock mass shocks. Figure 2 shows the location of the analysed dynamic shocks in relation to the progress of the wall over a period of about 6 months of the wall's operation. However, Figure 3 shows a map of the pressure distribution in the props of powered roof support from the same period.

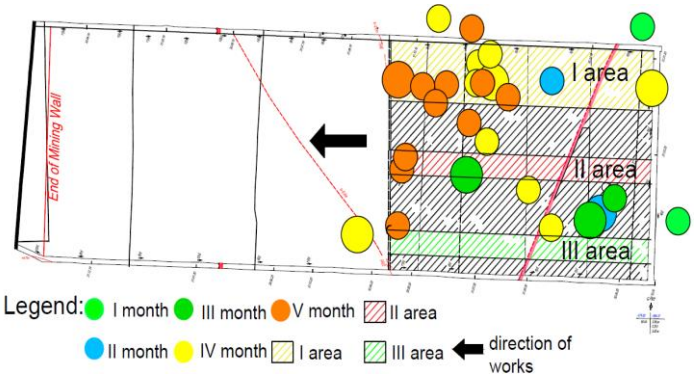


*Fig. 2. View from above. Location of the shocks in the area of the analysed wall and three research areas in the Coal Mine.*

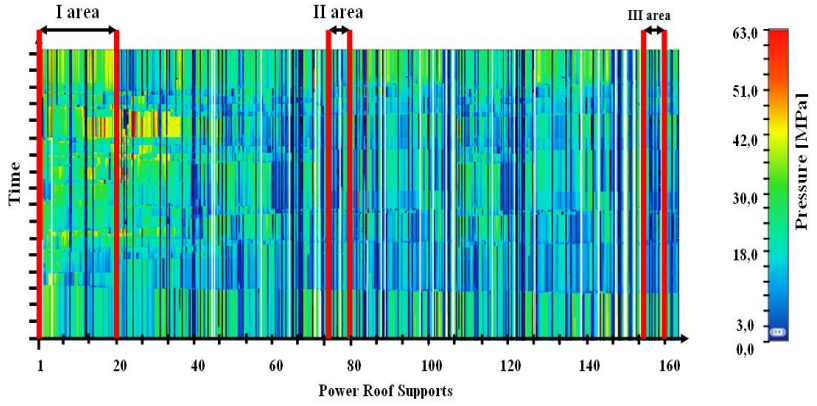


*Fig. 3. Map for the pressure distribution in the hydraulic props of the powered roof support from the area of the analysed wall along with the selected research areas.*

Figure 3 shows the three zones in relation to the pressure map. The figure shows the existing pressures in the roof support's props in reference to the passage of time. The example shows the previous month of the longwall exploitation. Based on measurement variables on the pressure map locations of the largest threats to the wall in operation have been predefined.

## Results and discussion

The selection of powered roof support depends on numerous parameters such as the coal and roof strength, the mining height and the capability of the roof. The method of identification of parameters affecting the load on the powered roof support in real conditions results from the direct pressure measurement. In order to determine the pressure changes occurring in the sub-piston space of the prop, a monitoring system was used. The research analysis focused only on measuring pressure during dynamic loading. Figure 4 shows the wireless pressure transducer.

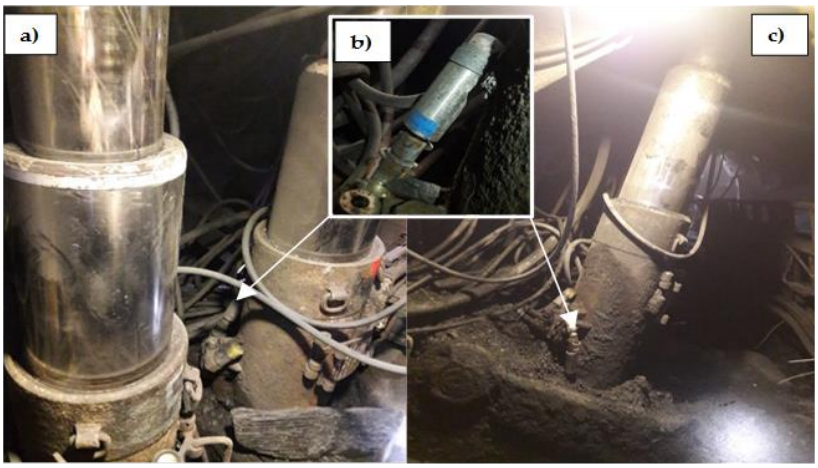


*Fig. 4. View of the measuring station in the mining wall, where: a -powered roof support from the front, b - pressure transducer type DROPS-01 OBAC17/ATEX0027X, c - powered roof support from the side of the workers' passage.*

The measuring system used consisted of pressure sensors of the DROPS-01 type, which communicate with each other wirelessly. The wireless signal goes to the converter, which is a local database for data from the system. The converter is equipped with radio circuits and a cable interface for communication with the computer. The computer located in the underground excavation is a local data server. The software visualises and analyses data from sensors on an ongoing basis. It has the ability to archive data, network diagnosis, reporting and viewing historical data. All information is sent to the surface using the mine's telephone network or optical fibre. The dispatch position on the surface has access to the data server. The task of dispatchers is to analyse and report on the basis of data obtained from sensors (Szurgacz, et al., 2020). To illustrate the work, the system is presented with a diagram of the measuring system, which is shown in Figure 5.

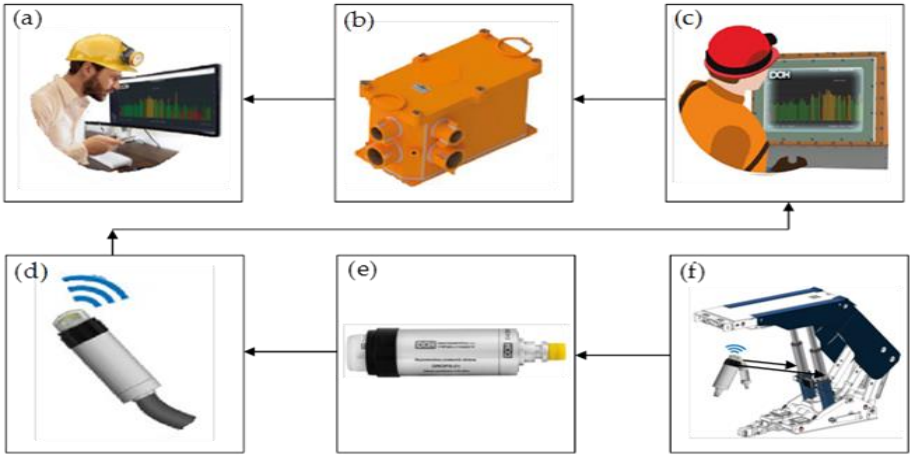


*Fig. 5. Scheme of the measuring system, where: (a) control stand, (b) underground transmission converter, (c) underground transmission converter, (d) intrinsically safe radio converter DILER-01, (e) wireless pressure transmitter type DOH DROPSY-01, (f) powered roof support.*

The obtained pressure measurements for the sub-piston space of the hydraulic prop of the powered roof support during the dynamic rock mass events are shown in Figure 6. The pressure variables that are shown in Figure 6, the pressure map and the location of shocks were all used to designate research areas. The location of the measuring zone in the area of the extraction longwall (Fig. 2) was intended to indicate the difference between the pressure increase and the change in its operation. The pressure changes during the rock mass shock were recorded for one representative section of the powered roof support. Figure 7 shows the pressure values after the first month of wall operation. Subsequent measurements (Fig. 8 and Fig. 9) show the pressure increase during the resulting shocks.

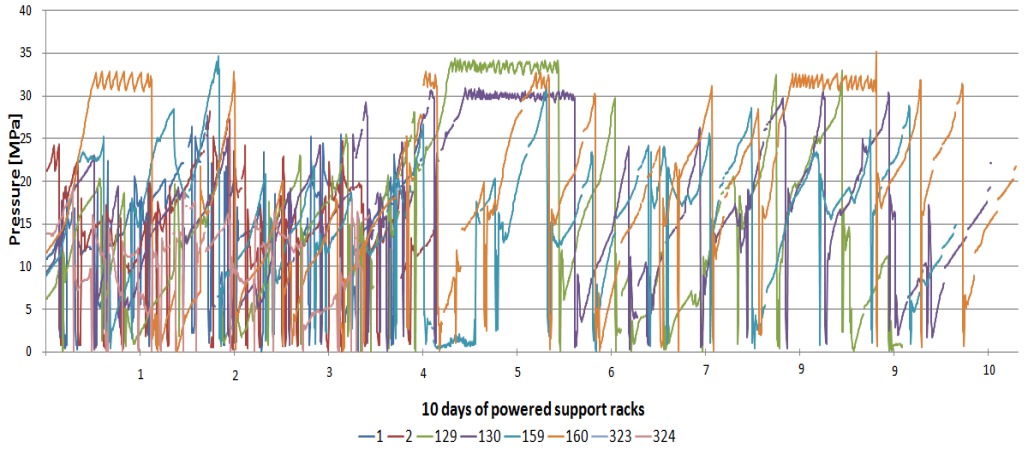


*Fig. 6. Distribution of the obtained pressure for selected sections of the powered roof support during the shock.*

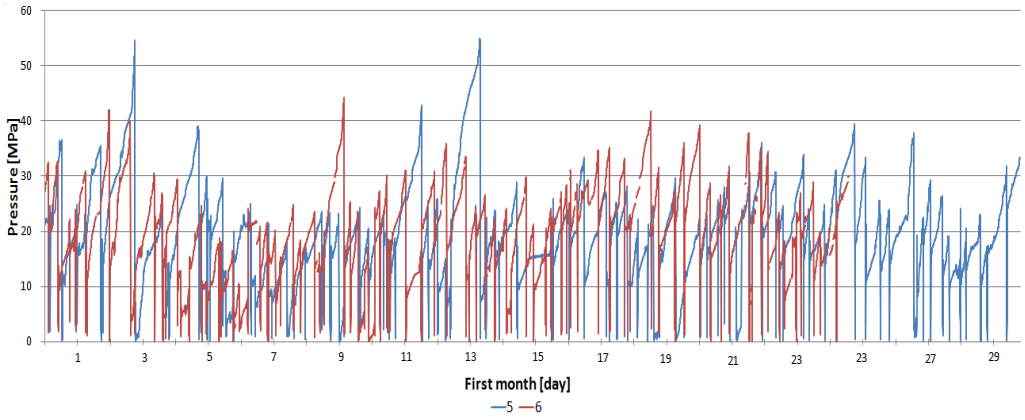


*Fig. 7. Distribution of the obtained pressure in the sub-piston space of the powered roof support's prop after the first month of wall operation.*

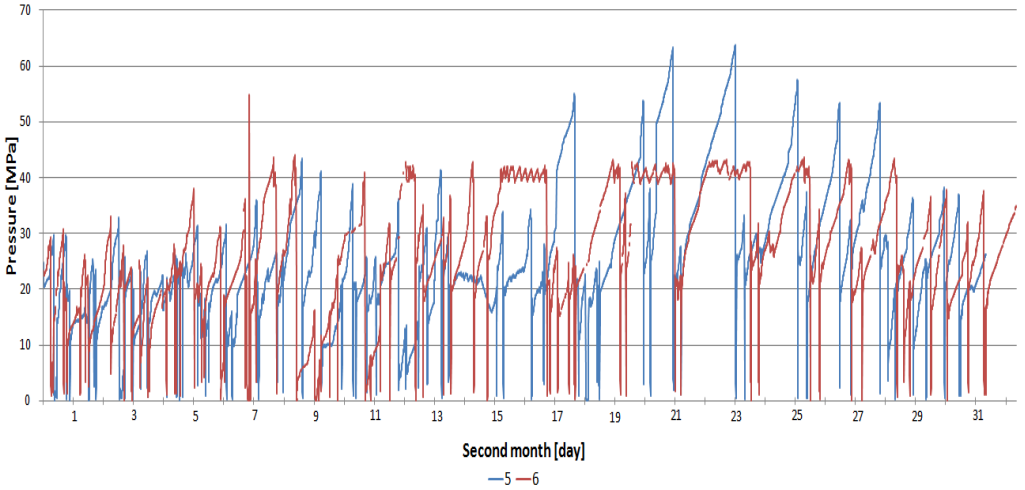


*Fig. 8. Distribution of the obtained pressure in the sub-piston space of the powered roof support's prop after the second month of wall operation.*

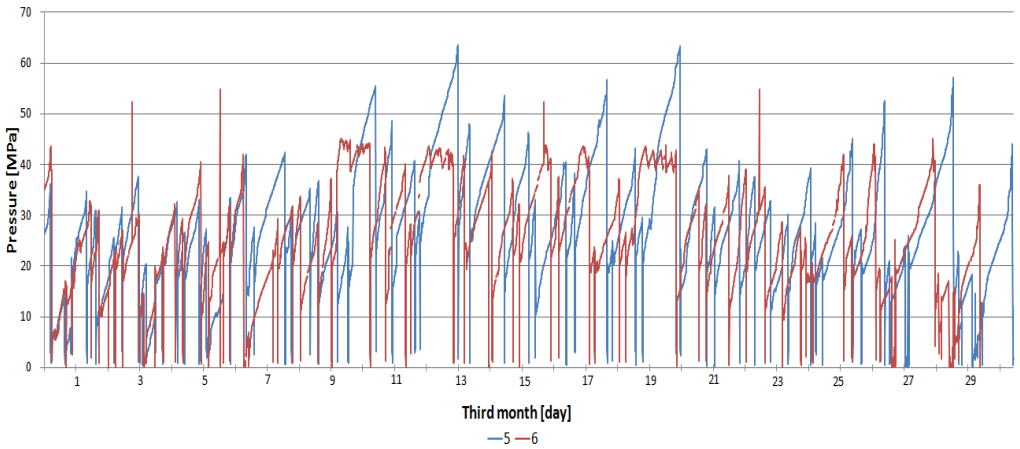


*Fig. 9. Distribution of the obtained pressure in the sub-piston space of the powered roof support's prop after the third month of wall operation.*

The analysis included 63 dynamic rock mass events in the designated three research zones of the longwall. A view of the measurement zones is shown in Figure 2. The first zone is the powered roof support sections from number 1 to number 20 (Figure 10-12). The second measuring zone is the powered roof support sections 74 to 80 (Fig. 13-15). Finally, the third measurement zone is the enclosure with numbers 154 to 160 (Fig. 16-18).

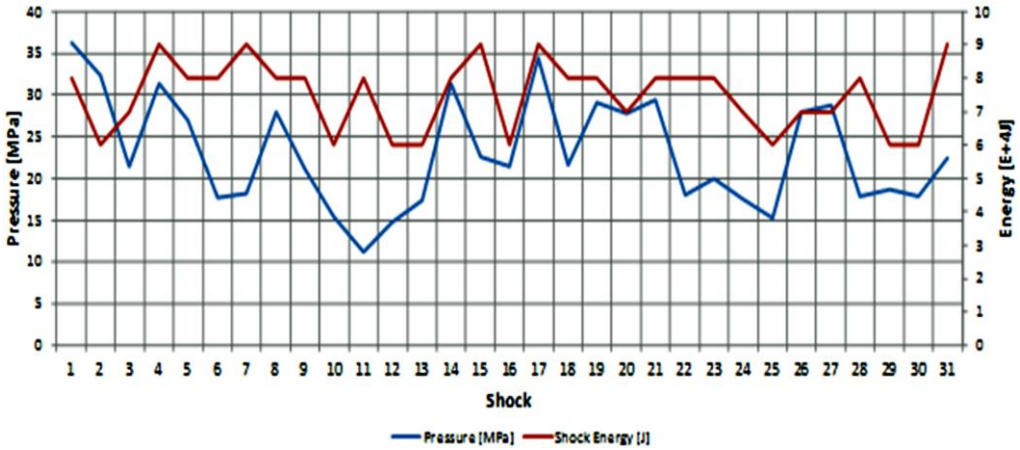


*Fig. 10. Analysis of the resulting pressure in the sub-piston space of the powered roof support's hydraulic prop and shock energy $10^4$J in the first test zone.*

The measurement (Fig. 10) shows the pressure variables for the registered 31 shocks during the longwall's operation. The maximum values were 37MPa for the energy $8x10^4$J. The minimum value occurred during the 11$^{th}$ shock and reached 12MPa at the energy of $8x10^4$J. The values pressures changed dynamically.

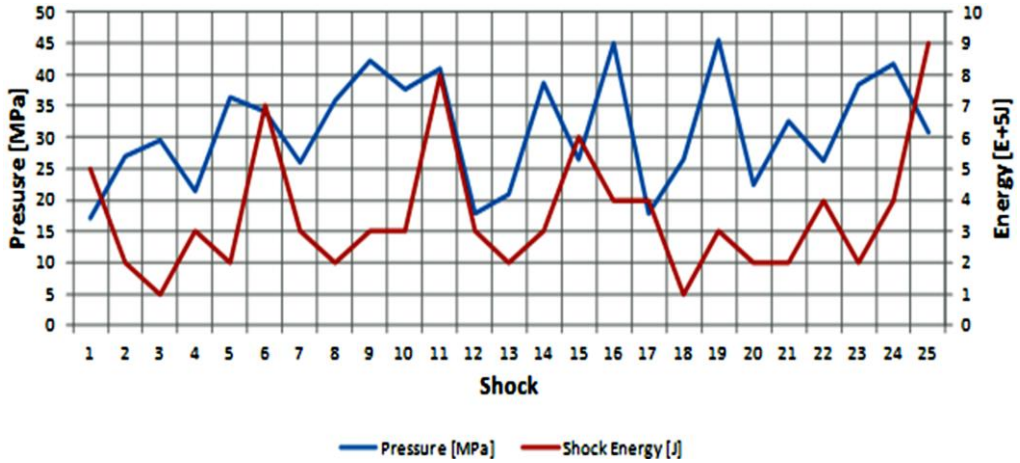


*Figure 11. Analysis of the resulting pressure in the sub-piston space of the powered roof support's hydraulic prop and shock energy $10^5$J in the first test zone.*

The obtained impact energy $10^5$J shows significant pressure fluctuations, reaching the highest values within the range of 45MPa (Fig. 11). The ratio of the occurring shocks shows a tendency to increase the pressure in the piston part of the prop. The highest value jump occurred during shocks 16 and 19.

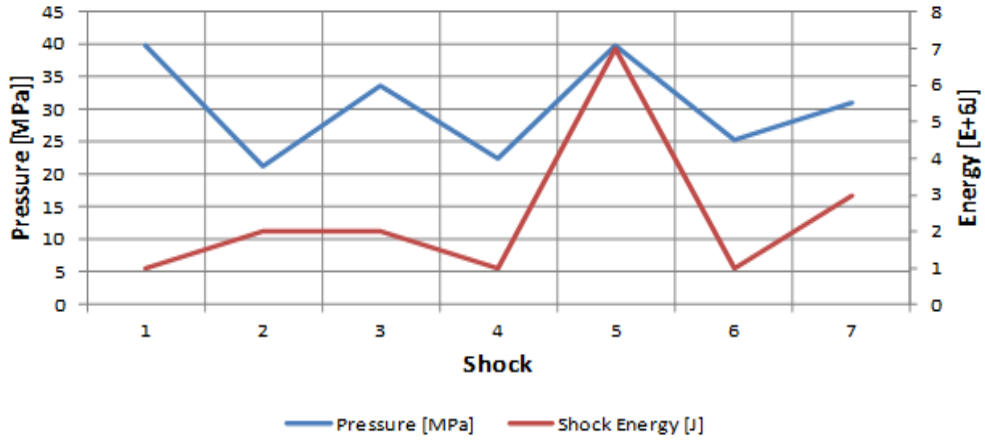


*Figure 12. Analysis of the resulting pressure in the sub-piston space of the powered roof support's hydraulic prop and shock energy $10^6$J in the first test zone.*

In the first zone, taking into account shocks of the order of $10^6$J, seven such cases were observed, which are presented in Figure No. 12. During the occurrence of shock 5, the highest pressure increase was recorded, reaching 40MPa. A significant increase in pressure in the prop is not always dependent on the amount of shock energy. Often, less energy generates higher pressure values. This phenomenon results from the properties of the surrounding rocks and the location of the shock.

The second zone is characterised by a significant increase in the value of pressures during 5-10 shocks for energy $10^4$J. In the area of 13-20 registered shocks, there was a pressure drop by 8MPa (fig. 13). Pressure variables ranged from 8MPa to 31MPa.

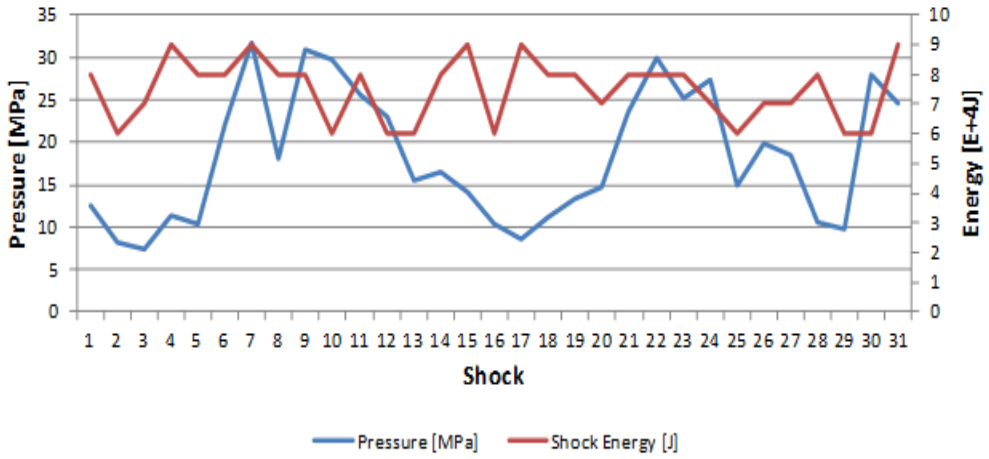


*Figure 13. Analysis of the resulting pressure in the sub-piston space of the powered roof support's hydraulic prop and shock energy $10^4$J in the second test zone.*

Figure No. 14 shows the pressure variables in the second zone for energy $10^5$J. The values retained the limits of 36MPa in the case of 25 high-energy shocks occurring in the longwall. The dynamic increase in pressure was characterised by shocks 16-19.

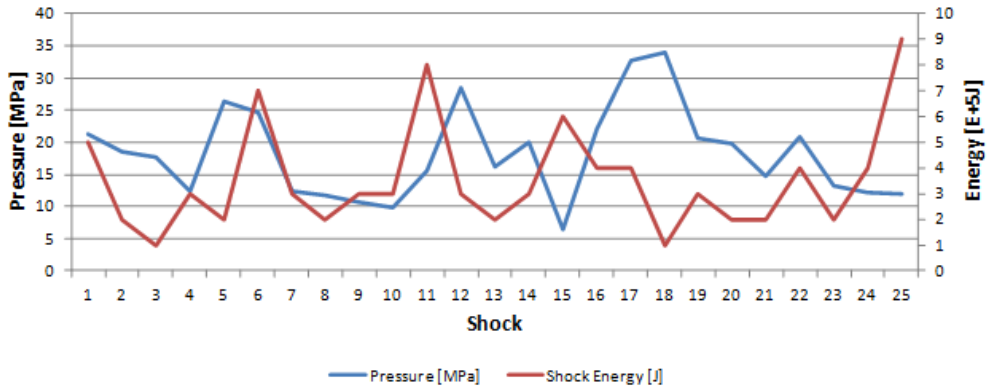


*Figure 14. Analysis of the resulting pressure in the sub-piston space of the powered roof support's hydraulic prop and shock energy $10^5$J in the second test zone.*

Figure 15 shows the pressure variables for seven shocks with an energy of $10^6$J for the third tested zone. From 1-3 shocks, pressure values increase dynamically for energy $2x10^6$J, but between 4-5 shocks decrease during energy $7x10^6$J. There is a significant increase for subsequent shocks, but the values do not exceed the limits of 30MPa.

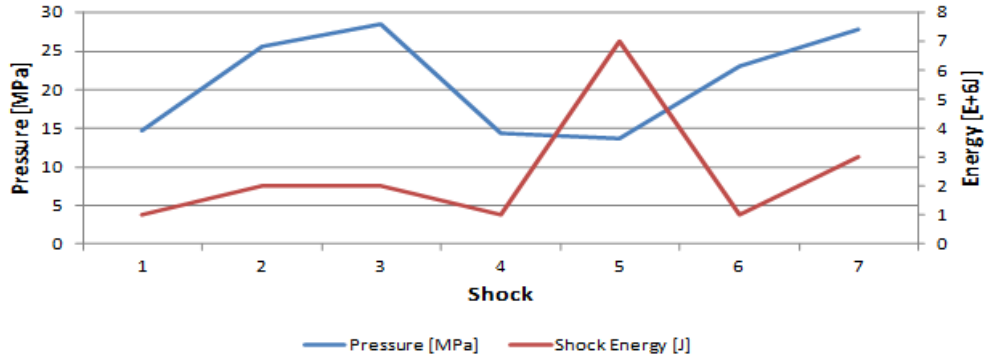


*Figure 15. Analysis of the resulting pressure in the sub-piston space of the powered roof support's hydraulic prop and shock energy $10^6$J in the second test zone.*

The obtained measurement (Fig. 16) in the third tested zone for energy $10^4$J is characterised at the initial stage by a relatively constant pressure variable with a difference of 5MPa. For subsequent shocks from 10 to 31, there are significant value changes within 15MPa

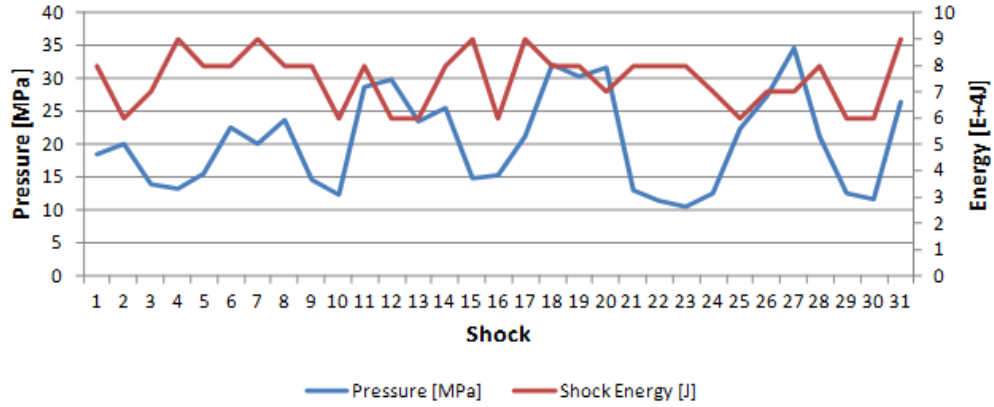


*Figure 16. Analysis of the resulting pressure in the sub-piston space of the powered roof support's hydraulic prop and shock energy $10^4$J in the third test zone.*

The measurement shown in figure 17 shows the pressure variables concerning the occurring shocks. Still, in this case, one can notice the dependence of low energy values that generate low-pressure values compared to the previous zones.

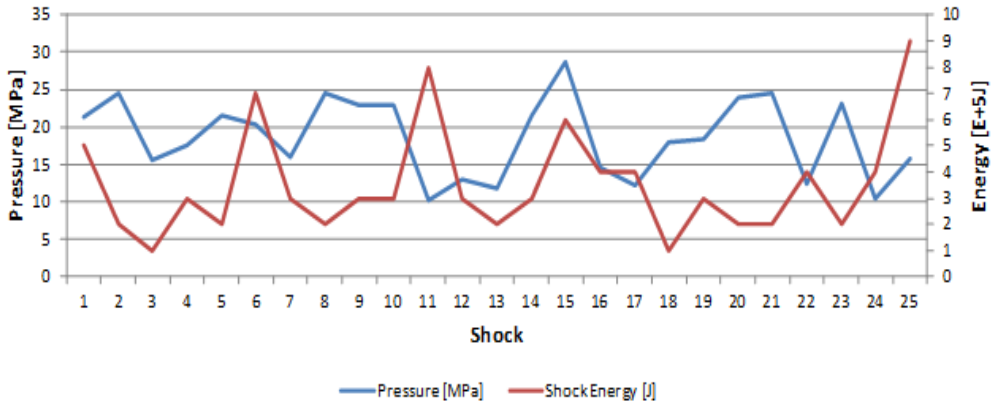


*Figure 17. Analysis of the resulting pressure in the sub-piston space of the powered roof support's hydraulic prop and shock energy $10^5$J in the third test zone.*

The above graph (fig. 18) shows seven shocks with an energy of $10^6$J for the third research zone. The value of pressure increased with subsequent shocks recorded in this area. During the 5$^{th}$ shock, where the energy reached the highest value, the pressure values in the section's props were reduced in the third zone.

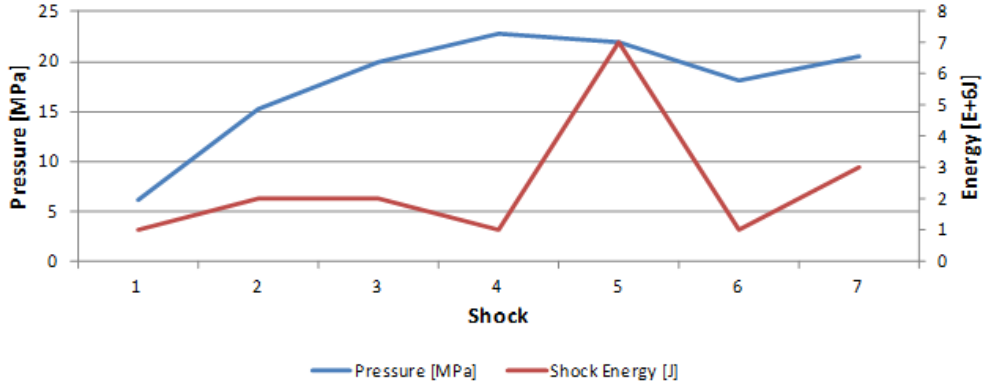


*Figure 18. Analysis of the resulting pressure in the sub-piston space of the powered roof support's hydraulic prop and shock energy $10^6$J in the third test zone.*

Based on the pressure and shock energy measurements in Tables 1-3 for the three test zones, the most significant values were selected to obtain the relation $P_{av}$ presented in the second chapter. Figures 19-25 illustrate the results in Tables 1-3.

*Tab. 1. The resulting shock energy with the obtained pressure in the sub-piston space of the powered roof support's prop for the first zone.*

| L.p. | Energy $10^4$J | $P_{max}$ [MPa] | $P_{av}$ | Energy $10^5$J | $P_{max}$ [MPa] | $P_{av}$ | Energy $10^6$J | $P_{max}$ [MPa] | $P_{av}$ |
|---|---|---|---|---|---|---|---|---|---|
| 1 | 8x$10^4$J | **36,26** | 37,13 | 5x$10^5$J | 17,16 | 27,58 | 1x$10^6$J | 39,8 | 38,9 |
| 2 | 6x$10^4$J | 32,3 | 35,15 | 2x$10^5$J | 27,1 | 32,55 | 2x$10^6$J | 21,24 | 29,62 |
| 3 | 7x$10^4$J | 21,4 | 29,7 | 1x$10^5$J | 29,5 | 33,75 | 2x$10^6$J | 33,64 | 35,82 |
| 4 | 9x$10^4$J | 31,35 | 34,67 | 3x$10^5$J | 21,31 | 29,65 | 1x$10^6$J | 22,4 | 30,2 |
| 5 | 8x$10^4$J | 26,97 | 32,48 | 2x$10^5$J | **36,4** | 37,2 | 7x$10^6$J | **39,8** | 38,9 |
| 6 | 8x$10^4$J | 17,76 | 27,88 | 7x$10^5$J | 34,2 | 36,1 | 1x$10^6$J | 25,26 | 31,63 |
| 7 | 9x$10^4$J | 18,18 | 28,09 | 3x$10^5$J | 25,9 | 31,95 | 3x$10^6$J | 30,92 | 34,46 |

*Tab. 2. The resulting shock energy with the obtained pressure in the sub-piston space of the powered roof support's prop for the second zone.*

| L.p. | Energy $10^4$J | $P_{max}$ [MPa] | $P_{av}$ | Energy $10^5$J | $P_{max}$ [MPa] | $P_{av}$ | Energy $10^6$J | $P_{max}$ [MPa] | $P_{av}$ |
|---|---|---|---|---|---|---|---|---|---|
| 1 | 8x$10^4$J | 12,6 | 25,3 | 5x$10^5$J | 21,22 | 29,61 | 1x$10^6$J | 14,65 | 26,32 |
| 2 | 6x$10^4$J | 8,25 | 23,12 | 2x$10^5$J | 18,45 | 28,22 | 2x$10^6$J | 25,63 | 31,81 |
| 3 | 7x$10^4$J | 7,39 | 22,69 | 1x$10^5$J | 17,6 | 27,8 | 2x$10^6$J | **28,46** | 33,23 |
| 4 | 9x$10^4$J | 11,45 | 24,72 | 3x$10^5$J | 12,36 | 25,18 | 1x$10^6$J | 14,44 | 26,22 |
| 5 | 8x$10^4$J | 10,31 | 24,15 | 2x$10^5$J | **26,29** | 32,14 | 7x$10^6$J | 13,65 | 25,82 |
| 6 | 8x$10^4$J | 22,08 | 30,04 | 7x$10^5$J | 24,6 | 31,3 | 1x$10^6$J | 23,03 | 30,51 |
| 7 | 9x$10^4$J | **31,79** | 34,89 | 3x$10^5$J | 12,41 | 25,20 | 3x$10^6$J | 27,78 | 32,89 |

*Tab. 3. The resulting shock energy with the obtained pressure in the sub-piston space of the powered roof support's prop for the third zone.*

| L.p. | Energy $10^4$J | $P_{max}$ [MPa] | $P_{av}$ | Energy $10^5$J | $P_{max}$ [MPa] | $P_{av}$ | Energy $10^6$J | $P_{max}$ [MPa] | $P_{av}$ |
|---|---|---|---|---|---|---|---|---|---|
| 1 | 8x$10^4$J | 18,6 | 28,3 | 5x$10^5$J | 21,26 | 29,63 | 1x$10^6$J | 6,19 | 22,09 |
| 2 | 6x$10^4$J | 20,02 | 29,01 | 2x$10^5$J | **24,58** | 31,29 | 2x$10^6$J | 15,26 | 26,63 |
| 3 | 7x$10^4$J | 14,01 | 26,00 | 1x$10^5$J | 15,68 | 26,84 | 2x$10^6$J | 19,94 | 28,97 |
| 4 | 9x$10^4$J | 13,2 | 25,6 | 3x$10^5$J | 17,52 | 27,76 | 1x$10^6$J | **22,77** | 30,38 |
| 5 | 8x$10^4$J | 15,6 | 26,8 | 2x$10^5$J | 21,45 | 29,72 | 7x$10^6$J | 21,89 | 29,94 |
| 6 | 8x$10^4$J | **22,6** | 30,3 | 7x$10^5$J | 20,4 | 29,2 | 1x$10^6$J | 18,1 | 28,05 |
| 7 | 9x$10^4$J | 20,11 | 29,05 | 3x$10^5$J | 15,89 | 26,94 | 3x$10^6$J | 20,45 | 29,22 |

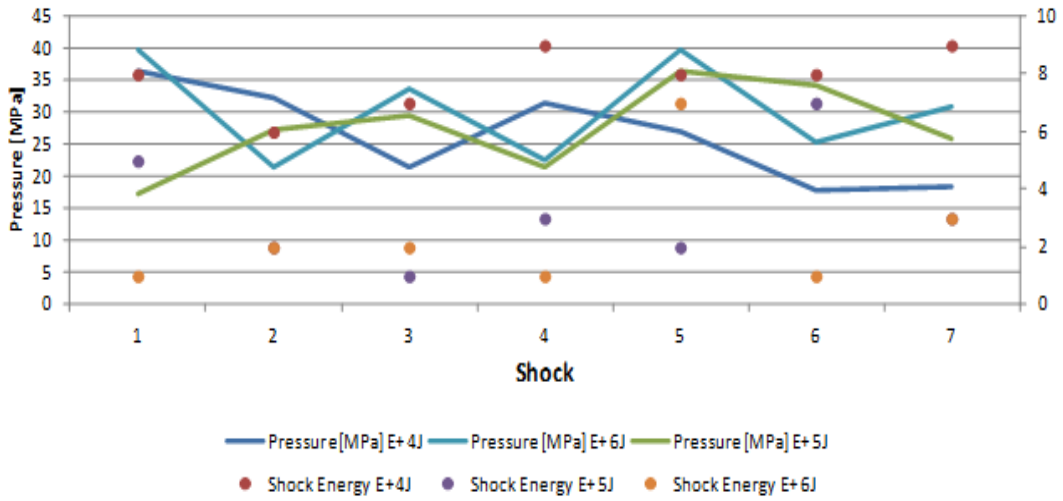


Fig. 19. The resulting shock energy with the obtained pressure in the sub-piston space of the powered roof support's prop for the first zone.

The measurement (fig. 19) presents significant changes in the pressure values in the first zone with the occurring shock energy from $10^4$J to $10^6$J. The highest recorded pressure value was 38.9MPa at $10^6$J during 1 and 5 high-energy shocks. The lowest values were recorded at energy $10^5$J with a value of 17,2 MPa.

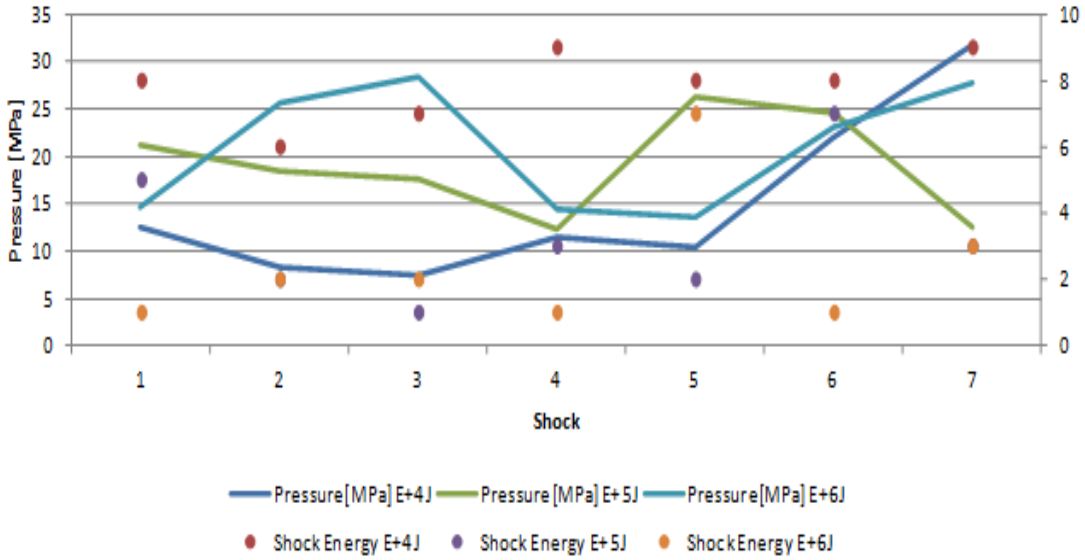


*Fig. 20. The resulting shock energy with the obtained pressure in the sub-piston space of the powered roof support's prop for the second zone.*

The second reaction zone was characterised by large amplitudes of pressure values, shown in Figure 20. The highest achieved pressure reached 31.8MPa. In the case of changes in the pressure values for the shock energy $10^4$J reached an increase of approx. 20.0MPa. The pressure for the energy $10^6$J during the 4th tested shock decreased sharply, maintaining a downward trend during the next shock. In the case of shocks 6 and 7, the pressure increased to 27.8MPa.

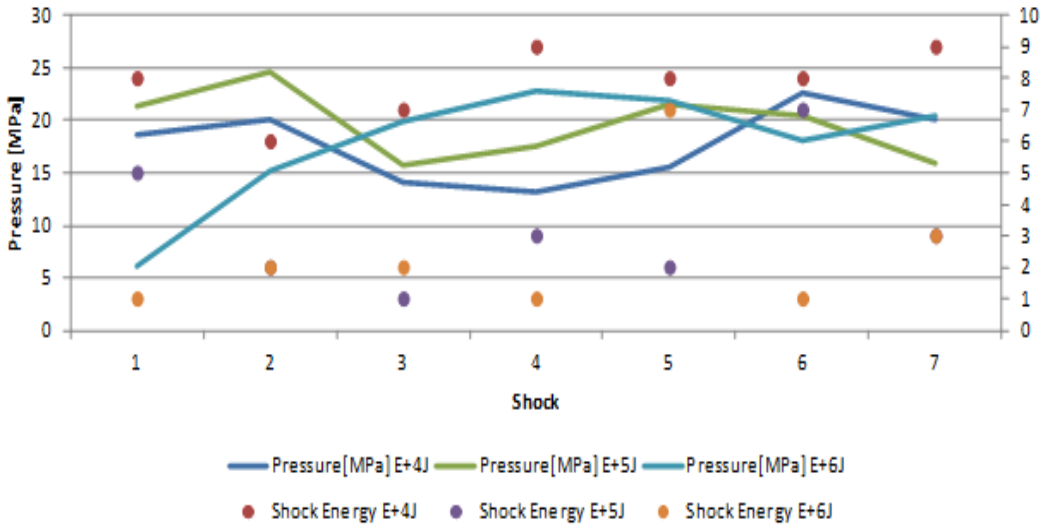


*Fig. 21. The resulting shock energy with the obtained pressure in the sub-piston space of the powered roof support's prop for the third zone*

In the third zone (Fig. 21), the pressure values were lower in relation to the first tested zone by approx. 8MPa. The third zone had stable pressure values for high-energy shocks. Pressures for energy $10^4$J increased gradually. The pressure values reached the maximum during the energy $10^5$J and $10^6$J, but during the subsequent two shocks, they dropped about 5MPa. The changes are shown in drawing no. 21.

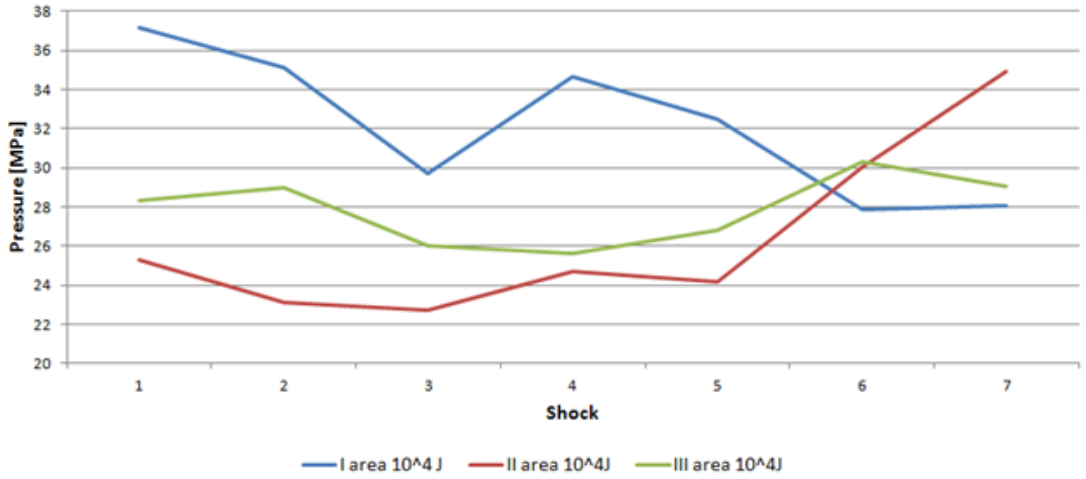


*Fig. 22. Analysis of the mean liquid pressure for the submarine space during rock tremors $10^4$ J for three test zones.*

Figure 22 shows the variable pressure values for the analysed three zones of the wall excavation. In this case, the energy of the order of $10^4$J was considered. The pressure values presented for each zone show significantly higher values for the first one. The phenomenon persists for the first five shocks, but during shocks 6 and 7, there is a dynamic increase in the pressure in the props for the second zone. The designated zones allowed us to assume the boundary conditions for the analysis. The zones were determined on the basis of a preliminary analysis of the location of shocks and variable pressure values.

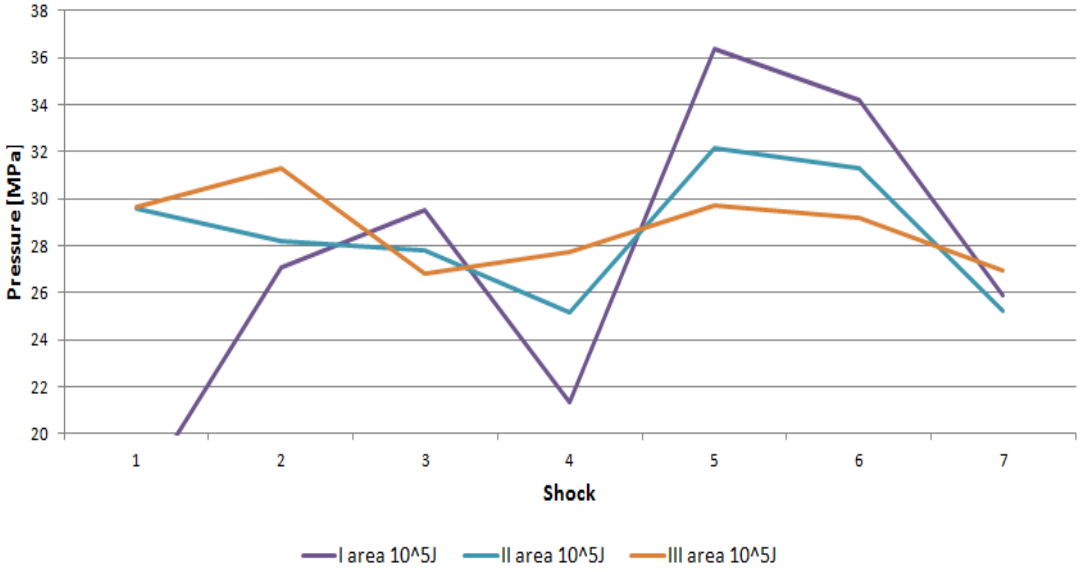


*Fig. 23. Analysis of the mean liquid pressure for the submarine space during rock tremors $10^5$J for three test zones.*

Figure 23 shows the occurrence of a shock of energy $10^5$J in the three zones. In this case, the first zone showed a dynamic pressure increase and a significant decrease by 10MPa at the occurrence of 4 shocks. The second and third zones were characterised by a stable value of pressures for the analysed seven high-energy shocks.

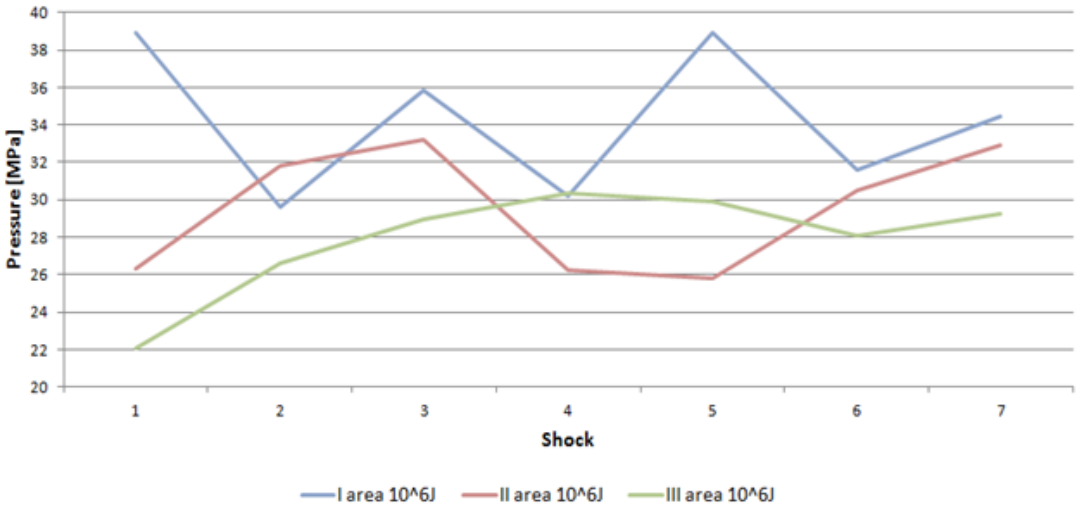


*Fig. 24. Analysis of the mean liquid pressure for the submarine space during rock tremors $10^6$ J for three test zones*

The three analysed (fig. 24) zones for energy $10^6$J reached different average pressure values. In the first zone, dynamic jumps and drops in moderate pressure can be seen, reaching even the value of 38.9MPa. For the second zone, the increase occurred for the first three shocks, followed by a pressure drop and another for shock 6. The third zone had a successive increase in average pressure, regulating at the level of approx 30.0MPa

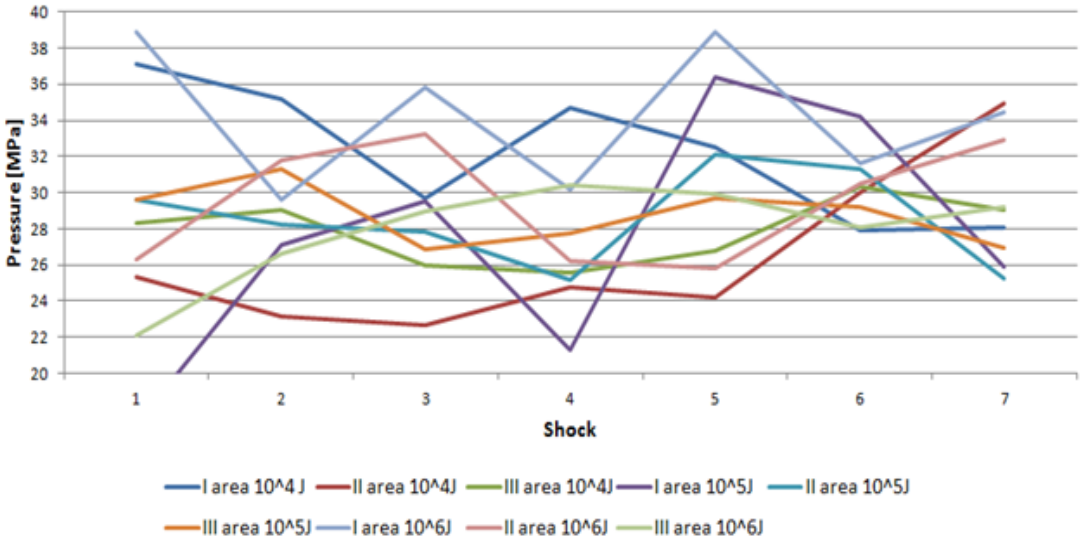


*Fig. 25. Analysis of the average liquid pressure for the sub-piston space during rock mass shock for three test zones.*

Figure 25 shows the variables of average pressure calculated based on the formula proposed by the authors in relation to the occurrence of energy shocks of the order of $10^4$J, $10^5$J, $10^6$J. Shock No. 4 is characteristic as each zone shows a significant drop in average pressures. The highest average value was 39MPa the lowest was 22MPa

## Conclusions

Using the prop's liquid pressure monitoring system, the data from the measurements under in situ conditions were analysed. The applied DROPS-01 type system measured the pressure with an accuracy of 0.1MPa with the frequency of a second in each of the stands of the powered roof support in the tested zone. The system consisted of pressure transducers installed on the housing stands (Fig. 2), a radio converter for communication between the transducer and the underground computer, and a downstream station for data transmission to the surface via optical fibre. Based on data analysis from sensors and shock registration, the areas in the wall were determined (Fig. 2) as most exposed to changes in the environment of the powered roof support. The data allowed us to generate a map of the pressure distribution (Fig. 3) and graphs of variable values of liquids in the powered roof support's props (Fig. 6-9). The pressure distribution map had increased pressure values in the powered roof support's props in the first designated wall zone. The rock mass shocks cause variable pressure values, which are shown in diagrams No. 10-25. The shock phenomenon significantly affects the operation of hydraulic props, causing damage and

disturbances in the operation of the powered roof support. The analysis covered the entire area of the wall's function; however, the paper presents three selected zones. The obtained results of pressure changes in the sub-piston space made it possible to illustrate the impact of the rock mass during high-energy shocks.

The analysed operation of the powered roof support's parameters monitoring system in relation to 63 high-energy shocks showed changes in pressure values in 75% of cases. According to observations, the remaining lack of registration in 15% was caused by the variable operating cycle of the powered roof support, system specifications, location of the shock and the direction of the seismic waves propagation. The designated research zones allowed us to focus on a detailed analysis of the recorded high-energy shocks in relation to the energy generated and variable pressure values. Considering each tested zone individually, in terms of varying pressures, the system recorded in the zone I 48% of such cases, in the zone II 39%, in the zone III 28%.

The analysis shows that the used system of monitoring the powered roof support's operation allows broader forecasting and determining the additional direction of applying preventive measures to the walls under the risk of tremors. The system provides increased possibilities for ensuring operational safety and increasing the efficiency of powered support. In the study, the analysis made it possible to determine the changes that took place in the rock mass before the shock. The pressure of the surrounding rocks changed with the cycle of the casing operation. The measurement of these values allows you to adjust the way of work and the speed of the wall moving towards the carbon to the prevailing conditions.

The system will improve the safety and efficiency of the walls after taking into account additional geological and mining factors and the way of cooperation with supporting systems. Predicting the occurrence of a rock mass shock with 100% certainty is not possible for now. However, the forecasting method is possible to achieve if the variables occurring in the liquid pressure of the powered roof support's props of the longwall are taken into account. Based on these values, we can determine the phenomenon of changes in the structure of surrounding rocks.

The presented analysis broadens the current knowledge about the possibility of using the powered roof support monitoring system. Using the monitoring system to observe changes in the rock mass before and after the shock allows taking measures in advance to reduce the risk of collapse or trembling.

## References


Baiul, K., Khudyakov, A., Vashchenko, S., Krot, P.V., and Solodka, N. (2020). The experimental study of compaction parameters and elastic after-effect of fine fraction raw materials. *Mining Science*, 27, 7–18. https://doi.org/10.37190/msc202701

Bajda, M., and Hardygóra, M. (2021). Analysis of Reasons for Reduced Strength of Multiply Conveyor Belt Splices. *Energies*, 14, 1512. https://doi.org/10.3390/en14051512

Bajda, M., Błażej, R., and Hardygóra, M. (2018). Optimizing Optimising splice geometry in multiply conveyor belts with respect to stress in adhesive bonds. *Mining Science*, 25, 195–206. https://doi.org/10.5277/msc182514

Bardzinski, P., Jurdziak, L., Kawalec, W., and Król, R. (2020). Copper ore quality tracking in a belt conveyor system using simulation tools. *Natural Resources Research*, 29(2), 1031-1040. doi:10.1007/s11053-019-09493-6

Bazaluk, O., Slabyi, O., Vekeryk, V., Velychkovych, A., Ropyak, L., and Lozynskyi, V. (2021). A Technology of Hydrocarbon Fluid Production Intensification by Productive Stratum Drainage Zone Reaming. *Energies*, 14, 3514. https://doi.org/10.3390/en14123514

Bazaluk, O., Velychkovych, A., Ropyak, L., Pashechko, M., Pryhorovska, T., and Lozynskyi, V. (2021). Influence of Heavy Weight Drill Pipe Material and Drill Bit Manufacturing Errors on Stress State of Steel Blades. *Energies*, *14*, 4198. https://doi.org/10.3390/en14144198

Borkowski, P.J. (2021). Comminution of Copper Ores with the Use of a High-Pressure Water Jet. *Energies*, 13, 6274. https://doi.org/10.3390/en13236274

Bortnowski, P., Gladysiewicz, L., Król, R., and Ozdoba, M. (2021). Tests of Belt Linear Speed for Identification of Fritional Contact Phenomena. *Sensors*, *20(20)*,5816. https://doi.org/10.3390/s20205816

Bortnowski, P., Gładysiewicz, L., Król, R., and Ozdoba, M. (2021). Energy efficiency analysis of copper ore ball mill drive systems. *Energies*, 14(6). doi:10.3390/en1406178.

Buyalich, G., Buyalich, K., and Byakov, M. (2017). Factors Determining the Size of Sealing Clearance in Hydraulic Legs of Powered Supports. *E3S Web Conf.*, 21, 3018

Buyalich, G., Byakov, M., and Buyalich, K. (2017). Factors Determining Operation of Lip Seal in the Sealed Gap of the Hydraulic Props of Powered Supports. *E3S Web Conf.*, 41, 1045.

Buyalich, G., Byakov, M., Buyalich, K., and Shtenin, E. (2019). Development of Powered Support Hydraulic Legs with Improved Performance. *E3S Web Conf.*, 105, 3025.

Dlouhá, D., and Hamříková, R. (2018). Interactive distance materials of mathematics for VŠB-TU Ostrava. *In Overcoming the Challenges and the Barriers in Open Education*, DisCo, pp. 67-72, Praha: Centre for Higher Education Studies.

Dlouhá, D., and Kozlová, K. (2019). Knowledge assessment of student's high school mathematics. *In 17th Conference on Applied Mathematics*, volume 1 of APLIMAT, pp. 243-252, Bratislava.

Dlouhá, D., Dubovský, V., and Pospíšil, L. (2021). Optimal calibration of evaporation models against Penman-Monteith equatíon. *Water,*13(11).

Dlouhá, D., Pokorný, J., and Dlouhá, K. (2019). Necessity of knowledge about math in safety engineering. *In E-Learning: Unlocking the Gate to Education around the Globe*, DisCo, pp. 380-386, Praha: Center for Higher Education Studies.

Doroszuk, B., and Król, R. (2019). Analysis of conveyor belt wear caused by material acceleration in transfer stations. *Mining Science,* 26, 189-201. doi:10.5277/msc192615

Frith, RC. (2015). A holistic examination of the load rating design of longwall shields after more than half a century of mechanised longwall mining. *Int.J. of Min. Sci. and Tech.* **2015**, 26(2), 199-208

Gładysiewicz, L., Król, R., Kisielewski, W., and Kaszuba, D. (2017). Experimental determination of belt conveyors artificial friction coefficient. *Acta Montanistica Slovaca, 22*(2), 206-214.

Góralczyk, M., Krot, P., Zimroz, R., and Ogonowski, S. (2020). Increasing Energy Efficiency and Productivity of the Comminution Process in Tumbling Mills by Indirect Measurements of Internal Dynamics—An Overview. *Energies*, 13, 6735. https://doi.org/10.3390/en13246735

Grzesiek, A., Zimroz, R., Śliwiński, P., Gomolla, N., and Wyłomańska, A. (2021). A Method for Structure Breaking Point Detection in Engine Oil Pressure Data. *Energies*, 14, 5496. https://doi.org/10.3390/en14175496

Hu, S., Ma, L., Guo, J. and, Yang, P. (2018). Support-surrounding rock relationship and top-coal movement laws in large dip angle fully-mechanized mechanised caving face. *Int.J. of Min. Sci. and Tech.*, 28(3), 533-539.

Huang, P., Spearing, S., Ju, F., Jessu, K.V., Wang, Z., and Ning, P. (2019). Control Effects of Five Common Solid Waste Backfilling Materials on In Situ Strata of Gob. *Energies*, 12, 154. https://doi.org/10.3390/en12010154

Ji, Y., Ren, T., Wynne, P., Wan, Z., Zhaoyang, M., and Wang, Z. (2016). A comparative study of dust control practices in Chinese and Australian longwall coal mines. *Int.J. of Min. Sci. and Tech.*, 25(5), 687-706.

Ji, Y., Zhang, Y., Huang, Z., Shao, Z., Gao, Y. (2020). Theoretical analysis of support stability in large dip angle coal seam mined with fully-mechanized mechanised top coal caving. *Mining Science*, 27, 73–87. https://doi.org/10.37190/msc202706

Jixiong, Z., Spearing, A.J.S., Xiexing, M., Shuai, G., and Qiang, S. (2017). Green coal mining technique integrating mining-dressing-gas draining-backfilling-mining. *Int.J. of Min. Sci. and Tech.*, 27(2), 17-27.

Juárez-Ferreras, R., González-Nicieza, C., Menéndez-Díaz, A., Álvarez-Vigil, A.E., and Álvarez-Fernández M.I. (2008). Measurement and analysis of the roof pressure on hydraulic props in longwall. *International Journal of Coal Geology*, Volume 75, Issue 1, pp. 49-62. https://doi.org/10.1016/j.coal.2008.01.007

Kawalec, W., Suchorab, N., Konieczna-Fuławka, M., Król, R. (2020). Specific energy consumption of a belt conveyor system in a continuous surface mine. *Energies,* 13(19) doi:10.3390/en13195214

Klishin, V.I., and Klishin, S.V. (2010). Coal Extraction from Thick Flat and Steep Beds. *J. Min. Sci.*, 46, 149–159.

Kotwica, K., Stopka, G. and, Prostański, G. (2021). Study and Application of Asymmetrical Disk Tools for Hard Rock Mining. *Energies*,14(*7*),1826. https://doi.org/10.3390/en14071826

Kotwica, K., Stopka, G., Kalita, M., Bałaga, D., and Siegmund, M. (2021). Impact of Geometry of Toothed Segments of the Innovative KOMTRACK Longwall Shearer Haulage System on Load and Slip during the Travel of a Track Wheel. *Energies,* 14, 2720. https://doi.org/10.3390/en14092720

Krauze, K., Mucha, K., Wydro, T., and Pieczora, E. (2021). Functional and Operational Requirements to Be Fulfilled by Conical Picks Regarding Their Wear Rate and Investment Costs. *Energies*, 14, 3696. https://doi.org/10.3390/en14123696

Kumar, R., Singh, A.K., Mishra, A.K., and Singh, R. (2015). Underground mining of thick coal seams. *Int.J. of Min. Sci. and Tech.*, 25(6), 885-896.

Mo, S., Tutuk, K., and Saydam, S. (2019). Management of floor heave at Bulga Underground Operations – A case study. *Int.J. of Min. Sci. and Tech.*, 29(1), 73-78.

Patyk, M., Bodziony, P., and Krysa, Z. (2021). A Multiple Criteria Decision Making Method to Weight the Sustainability Criteria of Equipment Selection for Surface Mining. *Energies*, 14, 3066. https://doi.org/10.3390/en14113066

Peng, S.S., Feng, D., Cheng, J., and Yang, L. (2019). Automation in U.S. longwall coal mining: A state-of-the-art review. *Int.J. of Min. Sci. and Tech.*, 29(2), 151-159.

Pokorny, J., Dlouhá, D., and Kucera, P. (2016). Study of the necessity of use virtual origin in assessment of selected fire plume characteristics. *MM Science Journal*, pp.1424-1428, 2016.

Pokorny, J., Mozer,V., Malerova, L., Dlouhá, D., and Wilkinson, P. (2018). A simplified method for establishing safe available evacuation time based on a descending smoke layer. *Communications – Scientific Letters of the University of Zilina*, 20(2), pp.28-34.

Qiao, S., Zhang, Z., Zhu, Z., and Zhang, K. (2021). Influence of cutting angle on mechanical properties of rock cutting by conical pick based on finite element analysis. *J. Min. Sci*., 28, 161–173.

Rajwa, S., Janoszek, T., and Prusek, S. (2019). Influence of canopy ratio of powered roof support on longwall working stability – A case study. *Int.J. of Min. Sci. and Tech.*, 29(4), 591-598.

Ralston, J.C., Hargrave, C.O., and Dunn, M.T. (2017). Longwall automation: trends, challenges and opportunities. *Int.J. of Min. Sci. and Tech.*, 27(5), 733-739.

Ralston, J.C., Reid, D.C., Dunn, M.T., and Hainsworth, D.W. (2015). Longwall automation: Delivering enabling technology to achieve safer and more productive underground mining. *Int.J. of Min. Sci. and Tech.*, 25(6), 865-876.

Ren, H., Zhang, D., Gong, S., Zhou, K., Xi, Ch., He, M., and Li, T. (2021). Dynamic impact experiment and response characteristics analysis for 1:2 reduced-scale model of hydraulic support. *International Journal of Mining Science and Technology*, Volume 31, Issue 3, pp. 347-356. https://doi.org/10.1016/j.ijmst.2021.03.004

Stoiński, K., and Mika, M. (2003). Dynamics of Hydraulic Leg of Powered Longwall Support. *J. Min. Sci.*, 39, 72–77.

Szurgacz, D. (2021). Dynamic Analysis for the Hydraulic Leg Power of a Powered Roof Support. *Energies*, 14, 5715. https://doi.org/10.3390/en14185715

Szurgacz, D., Bazan, Ł., Trzop, K., and Diederichs, R. (2020). A wireless pressure parameters visualisation system of a powered roof support on the example of Polish mines. *Mining–Informatics, Automation and Electrical Engineering*, 58.

Szurgacz, D., Zhironkin, S., Cehlár, M., Vöth, S., Spearing, S., and Liqiang, M. (2021). A Step-by-Step Procedure for Tests and Assessment of the Automatic Operation of a Powered Roof Support. *Energies*, 14, 697. https://doi.org/10.3390/en14030697

Szurgacz, D., Zhironkin, S., Vöth, S., Pokorný, J., Spearing, A.J.S., Cehlár, M., Stempniak, M., and Sobik, L. (2021). Thermal Imaging Study to Determine the Operational Condition of a Conveyor Belt Drive System Structure. *Energies*, 14, 3258. https://doi.org/10.3390/en14113258

Wajs, J., Trybała, P., Górniak-Zimroz, J., Krupa-Kurzynowska, J., and Kasza, D. (2021). Modern Solution for Fast and Accurate Inventorization of Open-Pit Mines by the Active Remote Sensing Technique—Case Study of Mikoszów Granite Mine (Lower Silesia, SW Poland). *Energies*, 14, 6853. https://doi.org/10.3390/en14206853

Wang, J., and Wang, Z. (2021). Systematic principles of surrounding rock control in longwall mining within thick coal seams. *Int.J. of Min. Sci. and Tech.*, 29(1), 591-598.

Wodecki, J., Góralczyk, M., Krot, P., Ziętek, B., Szrek, J., Worsa-Kozak, M., Zimroz, R., Śliwiński, P., and Czajkowski, A. (2020). Process Monitoring in Heavy Duty Drilling Rigs—Data Acquisition System and Cycle Identification Algorithms. *Energies*, 13, 6748. https://doi.org/10.3390/en13246748

Woźniak, D., and Hardygóra, M. (2020). Method for laboratory testing rubber penetration of steel cords in conveyor belts. *Mining Science*, 27, 105–117. https://doi.org/10.37190/msc202708

Xiaozhen, W., Jialin, X., Weibing, Z., and Yingchun, Li. (2012). Roof pre-blasting to prevent support crushing and water inrush accidents. *Int.J. of Min. Sci. and Tech.*, 22(3), 379-384.

Zhao, X., Li, F., Li, Y., and Fan Y. (2015). Fatigue Behavior of a Box-Type Welded Structure of Hydraulic Support Used in Coal Mine. *Materials*, 8(10), 6609-6622. https://doi.org/10.3390/ma8105325

Zhou, R., Meng, L., Yuan, X., and Qiao, Z. (2022). Research and Experimental Analysis of Hydraulic Cylinder Position Control Mechanism Based on Pressure Detection. *Machines*, 10(1), 1. https://doi.org/10.3390/machines10010001

Ziętek, B., Banasiewicz, A., Zimroz, R., Szrek, J., and Gola, S. (2022). A Portable Environmental Data-Monitoring System for Air Hazard Evaluation in Deep Underground Mines. *Energies*, 13, 6331. https://doi.org/10.3390/en13236331

Zimroz, P., Trybała, P., Wróblewski, A., Góralczyk, M., Szrek, J., Wójcik, A., and Zimroz, R. (2021). Application of UAV in Search and Rescue Actions in Underground Mine—A Specific Sound Detection in Noisy Acoustic Signal. *Energies*, 14, 3725. https://doi.org/10.3390/en14133725